OPEN

Automated optimization of photonic crystal slab cavities

Momchil Minkov & Vincenzo Savona

Institute of Theoretical Physics, Ecole Polytechnique Fédérale de Lausanne EPFL, CH-1015 Lausanne, Switzerland.

Thanks to their high quality factor, combined to the smallest modal volume, defect-cavities in photonic crystal slabs represent a promising, versatile tool for fundamental studies and applications in photonics. In paricular, the L3, H0, and H1 defects are the most popular and widespread cavity designs, due to their compactness, simplicity, and small mode volume. For these cavities, the current best optimal designs still result in Q-values of a few times 10^5 only, namely one order of magnitude below the bound set by fabrication imperfections and material absorption in silicon. Here, we use a genetic algorithm to find a global maximum of the quality factor of these designs, by varying the positions of few neighbouring holes. We consistently find Q-values above one million – one order of magnitude higher than previous designs. Furthermore, we study the effect of disorder on the optimal designs and conclude that a similar improvement is also expected experimentally in state-of-the-art systems.

P hotonic crystal (PhC) cavities are a quintessential element of integrated photonic devices. Thanks to ultra-high quality factors and mode volumes close to the diffraction limit[1–13], these devices hold promise in a wide range of applications including non-classical light generation, all-optical computational paradigms, solid-state cavity quantum electrodynamics, and sensing[14–24]. Starting from a two-dimensional PhC consisting of a lattice of air holes etched in a dielectric slab, an optical cavity can be created by introducing a point-like defect – e.g. one or few missing or shifted holes – in the otherwise periodic structure.

A major effort during the last decade has been devoted to the optimization of these structures, in particular through the maximization of the quality factor Q and the minimization of the volume V of the cavity mode, as optical nonlinearities, Purcell effect, and radiation-matter coupling all depend directly on Q and inversely on V[25–28]. To this purpose, three different approaches can be broadly defined. The first is the inverse problem approach[3,4], where an effective equation for the dielectric profile is defined starting from the desired shape of the cavity mode, through a semi-analitical formalism. The second is the topology optimization method[29], where variations of the entire topology of the PhC are allowed, and the objective function (either Q or Q/V) is maximized numerically[30–32]. Although some of these works[3,32] have achieved remarkably high values of Q and Q/V, the resulting cavity designs often pose serious technological challenge in terms of manufacturability, as they present excessively small holes or holes with irregular pattern and sharp features. A third and completely different strategy consists in optimizing simple PhC cavity designs by tweaking only a few geometrical parameters (e.g. by shifting the positions and varying the radii of nearby holes), in order to preserve the small spatial footprint and ease of fabrication of the design. This approach has produced encouraging results, in particular for the three most widespread cavity designs, namely the L3 cavity[1,2,9,33], the H0 cavity (also known as "zero-cell" or "point-shift" cavity)[6,9], and the H1 cavity[8,9,11,13,34]. It brought in some cases an increase of the quality factor by more than one order of magnitude – reaching values of a few hundred-thousands, or even above one million for the H1 hexapole mode[11,13] – while the mode volume was only slightly increased or sometimes even reduced. A common feature of all these optimization works however is the lack of an exhaustive exploration of the parameter space in search of a global maximum of the objective function.

Experimentally, the quality factor of PhC cavities is limited by extrinsic losses, due to absorption and fabrica-tion imperfections[12,35–37]. More precisely, the measured quality factor Q_e can be expressed as

$$\frac{1}{Q_e} = \frac{1}{Q_t} + \frac{1}{Q_a} + \frac{1}{Q_d}, \tag{1}$$

where Q_t is the theoretical quality factor expected from the ideal structure, while $1/Q_a$ and $1/Q_d$ are measures of the additional loss rates due to material absorption and to disorder-induced extrinsic losses respectively. For silicon PhCs and wavelengths in the 1.5 μm range, record values of Q_e ranging between one and five million were

measured on cavity designs based on a modulation of a one-dimensional PhC waveguide[5,7,10–12]. For these designs, Q_t ranges between 2×10^7 and 10^8, suggesting a value of several millions for both Q_d and Q_a. While displaying a mode volume up to three times larger than that of defect cavities, these waveguide-based designs have a considerably larger footprint. There are no fundamental reasons that should prevent the quality factor of the most popular defect cavities from reaching values of several million, close to the current bound set by disorder and absorption.

Here, we adopt a simple optimization strategy. Similarly to several existing works[1,2,6,8,9,11,13,33,34], we choose a small set of variational parameters – typically the spatial shifts of a few holes next to the defect – thus producing designs that can be easily realized with current nanofabrication processes. Differently from these works however, we carry out a global exploration of the parameter space by means of an evolutionary algorithm. Here, by "global" we mean the exhaustive search for the global maximum of the quality factor in the parameter space of choice. In this way we demonstrate that it is possible to systematically optimize L3, H0, and H1 cavities to values of Q_t well above 10^6 – typically more than one order of magnitude above previous optimal values – without a large increase of the mode volumes. The key to this drastic improvement is the exhaustive search, that finds configurations overlooked by previous approaches, as exemplified by the simplest of the two L3 designs considered here[2]. This optimization procedure is made computationally feasible thanks to the use of the guided-mode expansion (GME) method[38], that allows calculation of the modes and quality factors of each variation within minutes of computational time. Thanks to this computational advantage, we also statistically analyze the influence of fabrication imperfections on the optimal designs and conclude that a considerable improvement in the *experimental* quality factor can be expected, as recently demonstrated for the H0 design[39].

Results

The cavities studied here are formed in a triangular lattice with pitch a of air-holes of radius R etched in a silicon ($n = 3.46$) slab of thickness d. In what follows, all lengths will be expressed in units of a, as the quality factor is invariant upon a spatial rescaling of the structure. We however set parameters such that, for the typically used thickness $d = 220$ nm, the resonant modes lie in the telecommunication band around $\lambda = 1.55$ μm. For the simulation of a single structure, we use the GME method[38] (see Methods). This method has already proven reliable for modelling high-Q cavities[35,37]. As a further check of its validity, the results for all final (optimized) structures are verified using the 3-D finite-difference time-domain (FDTD) method[40] (see Methods). For each of the optimized designs presented here, we also analyse the probability density of Q_e in the presence of fabrication imperfections (and neglecting the absorption loss contribution $1/Q_a$). The disorder model is that of Gaussian distributed random fluctuations in the position and radius of each hole, with zero mean and standard deviation σ (which is a measure of the disorder magnitude). Disorder in all holes in the computational cell was included, and no hole-hole correlations were taken into account. Irregular hole shapes can in general easily be included, but the resulting effect is well described by an effective radius fluctuation[41]. The disorder model thus captures well what is accepted as the main source of losses in silicon photonic crystal cavities[12,35,36].

The first cavity design we investigate is the widely-employed L3 cavity formed by three missing holes in a row (Fig. 1(a)), with $d = 0.55a$ and $R = 0.25a$. The quality factor of this cavity has already been optimized[2] with respect to shifts of the positions of three neighbouring holes (marked S_{1x}, S_{2x}, and S_{3x} in the Figure), by using a simplified approach in which, starting from the unshifted design, each of the three shifts has been varied once while keeping the two others constant. To explore the extent to which this approach is suitable, we compute a full map of the quality factor on a relevant region of the

(S_{1x}, S_{2x}, S_{3x})-space. The map is displayed in Fig. 1(b)–(m). There, in each panel, Q_t is plotted as a function of S_{2x} and S_{3x}, while the value of S_{1x} increases from $0.15a$ to $0.37a$ in steps of $0.02a$ when going from panel (b) to panel (m). Technically, these plots already provide a global optimization of the cavity (a clear maximum of Q_t can be identified), although performed in the least practical, brute-force way. If applied to the panels of Fig. 1 (though approximately, given the coarse S_{1x} step used in this figure), the simplified optimization procedure in Ref. 2 leads to the point marked by a white cross in panel (e) (more precisely, $S_{1x} = 0.21a$, $S_{2x} = 0.01a$, $S_{3x} = 0.23a$), i.e. far off the maximum that can be seen in panel (k) at $S_{1x} = 0.33a$, $S_{2x} = 0.26a$, $S_{3x} = 0.10a$. It is also interesting to note that within the range of the plots in Fig. 1(b–m), two maxima are visible - a local one around $S_{1x} = 0.25a$, $S_{2x} = 0.09a$, $S_{3x} = 0.21a$ in panel (g) and another one which first appears at $S_{1x} = 0.29a$, $S_{2x} = 0.18a$, $S_{3x} = -0.10a$ in panel (i) and then shifts to become the global maximum at $S_{1x} = 0.327a$, $S_{2x} = 0.257a$, $S_{3x} = 0.116a$. In general, an even larger number of local extrema might in principle be present, especially for larger number of parameters, thus making the search for the global extremum more difficult. This highlights the need for a global optimization procedure instead of a more conventional algorithm (e.g. the conjugate gradient) that would almost inevitably find a local rather than a global maximum.

Ideally, we would like to apply a global, stochastic (since there is no general way to come up with a "good" guess for a starting point) procedure to the problem of optimizing the cavity parameters. Thus, we choose to employ a genetic algorithm which typically relies on a range of evolution-inspired techniques to create consecutive "generations" of cavities each containing better and better "individuals", until convergence is reached. This type of algorithm proves very efficient especially with increasing number of free parameters. We use the genetic algorithm provided in the MATLAB® Global Optimization Toolbox (see Methods), where we choose the objective function to be the GME-computed quality factor Q_t. When applied to the L3 with freedom in S_{1x}, S_{2x} and S_{3x}, the optimal design is found for $S_{1x} = 0.327a$, $S_{2x} = 0.257a$ and $S_{3x} = 0.116a$ (Fig. 2(a)). This yields $Q_t = 2.1 \times 10^6$ (FDTD: 1.6×10^6), which is an increase by a factor of ≈ 6 as compared to the previously highest value[2] of 3.3×10^5 (FDTD: 2.6×10^5), while the mode volume (see Methods) increases from $0.77(\lambda/n)^3$ to $0.94(\lambda/n)^3$. One obvious advantage of using evolutionary optimization rather than the brute-force parameter scan of Fig. 1 is the precision with which the maximum can be pinpointed; another one is that a few tens of generations with a population of 80 individuals are sufficient to reach this converged configuration (see Methods). Moreover, the design can be further improved if two more shifts (S_{4x} and S_{5x} in Fig. 1(a)) are allowed in the optimization, which is still easily handled by the genetic algorithm, although ≈ 100 generations are needed for convergence. In this case, the optimized design is found for $S_{1x} = 0.337a$, $S_{2x} = 0.270a$, $S_{3x} = 0.088a$, $S_{4x} = 0.323a$, and $S_{5x} = 0.173a$ (Fig. 2(b)), and has $Q_t = 5.1 \times 10^6$ (FDTD: 4.2×10^6) with mode volume $V = 0.95(\lambda/n)^3$, i.e. an increase in Q_t by one order of magnitude compared to the previous optimal values[2,33], with an increase in the mode volume comparable to the three-shift case. The resonant frequency of the modes is at $\frac{\omega a}{2\pi c} = 0.259$ for both designs, which is slightly lower than the frequency $\frac{\omega a}{2\pi c} = 0.263$ of the unmodified L3 (i.e. with the same d/a and R/a but with no hole shifts).

The choice of just these few free parameters is not unique, but appears optimal. Attempts were made at including other position shifts or radii variations of the holes surrounding the cavity defect, which however did not bring to a significant further increase in Q_t. Having only a few hole shifts as free parameters results in a technologically friendly structure, and in a more compact cavity defect, characterized by a much smaller footprint on the PhC, than waveguide-based ultrahigh-Q designs[4,5,7]. In addition, the present designs

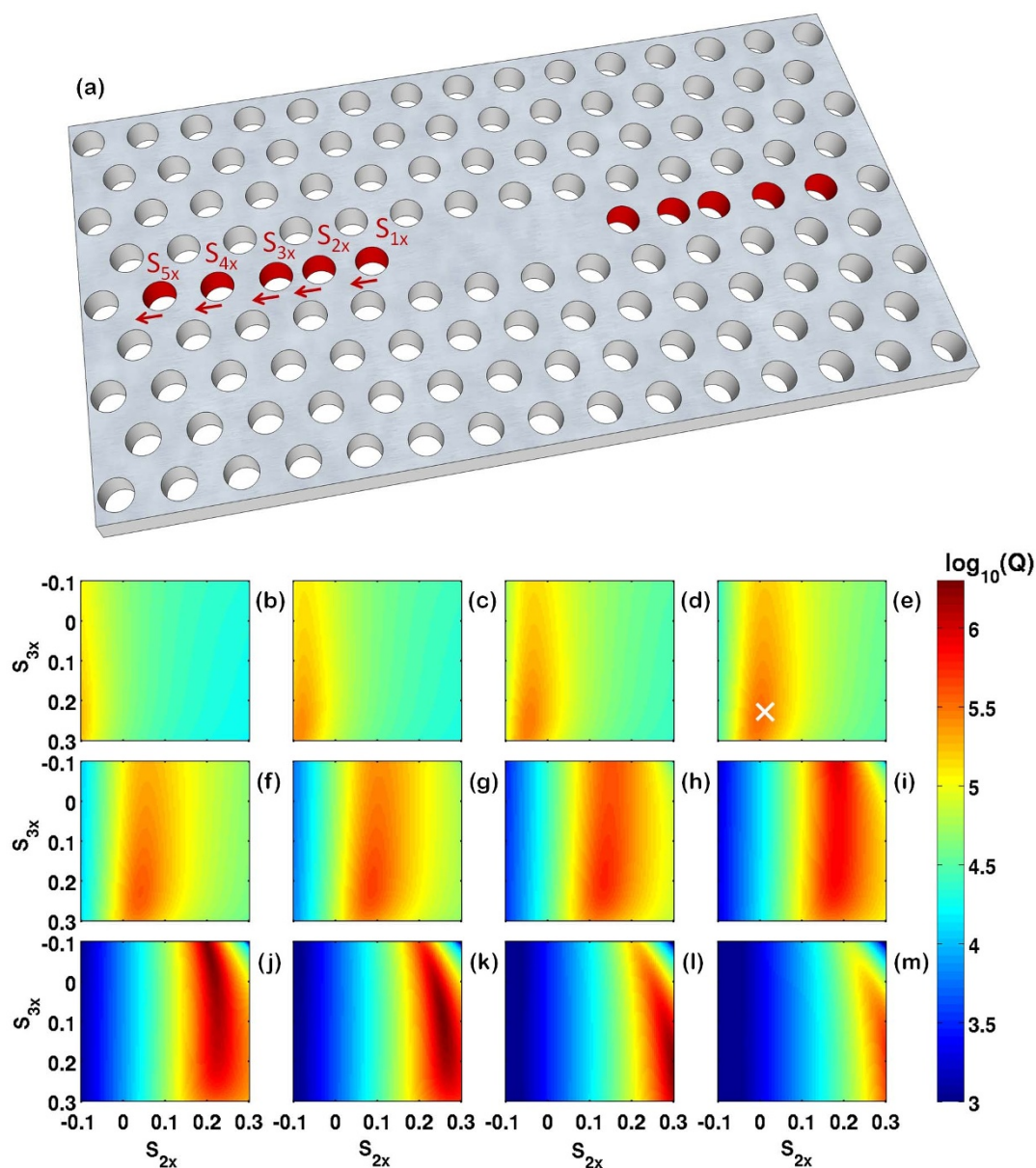**Figure 1** | (a): The design of the L3 cavity. For quality factor optimization, shifts of the positions of the five neighbouring holes in the x-direction were introduced, labeled as S_{1x}, S_{2x}, S_{3x}, S_{4x}, and S_{5x} in the figure. (b)–(m): A parameter scan of the GME-computed quality factor values for different S_{1x}, S_{2x} and S_{3x}, where S_{1x} starts from $0.15a$ in panel (b) and increases in multiples of $0.02a$ in every consecutive panel, up to $0.37a$ in (m), and $S_{4x} = S_{5x} = 0$ in all panels.

are as robust to fabrication imperfections as any other high-Q PhC cavity[37], as can be inferred from Fig. 2(c)–(f). In panel (c) we plot, for the three-shift L3, the dependence of Q_t on S_{2x} and S_{3x} as in Fig. 1, but for the value $S_{1x} = 0.327a$ corresponding to our optimal design (the white cross indicates where the design lies with respect to S_{2x} and S_{3x}). In this plot, we observe that the width of the maximum is larger than the typical uncertainty in the hole positions (smaller than $0.005a$ for Si[42]). Furthermore, in Fig. 2(d)–(e) we show, respectively, for the three- and five-shift design, the computed probability of occurrence of Q_e-values in presence of disorder. Each of these histograms was obtained by simulating 1000 disordered realisations of the corresponding cavity design. The blue plot in panel (d) in particular shows that for a state-of-the-art disorder magnitude $\sigma = 0.0015a$ (i.e. about 0.6 nm[12,35], when assuming $a = 400$ nm in a silicon slab), the average value lies at about $Q_e = 2.5 \times 10^6$, i.e. quality factors one order of magnitude larger than the previous *theoretical* maximum can be expected *in practice*, highlighting the significance of the design

optimization. Finally we note that, for a given set of optimal values of the S_{nx} parameters, the designs are also robust to small changes in the overall hole radius R and slab thickness d, that can originate from an offset in the fabrication process and/or be introduced on purpose in order to e.g. tune the resonant frequency to a desired value. To show this, in panel (f) we plot the value of Q_t obtained by varying R and d while keeping the shifts $S_{1x} - S_{5x}$ constant and set to the values obtained for the optimal design computed at $d = 0.55a$ and $R = 0.25a$. We observe that $Q_t > 4 \times 10^6$ for a range of R and d values which is much larger than the fabrication uncertainty and which allows fine-tuning of the frequency. For certain values of d and R (to the right of the dashed line in the Figure), higher-order guided modes of the slab become non-negligible. More precisely, a TM-like band of the regular PhC becomes resonant with the cavity mode and introduces a new loss channel[38]. We point out that, while Q_t appears to systematically increase with d in the single-mode region, it drops rapidly as soon as d increases into the multi-mode region. An ana-
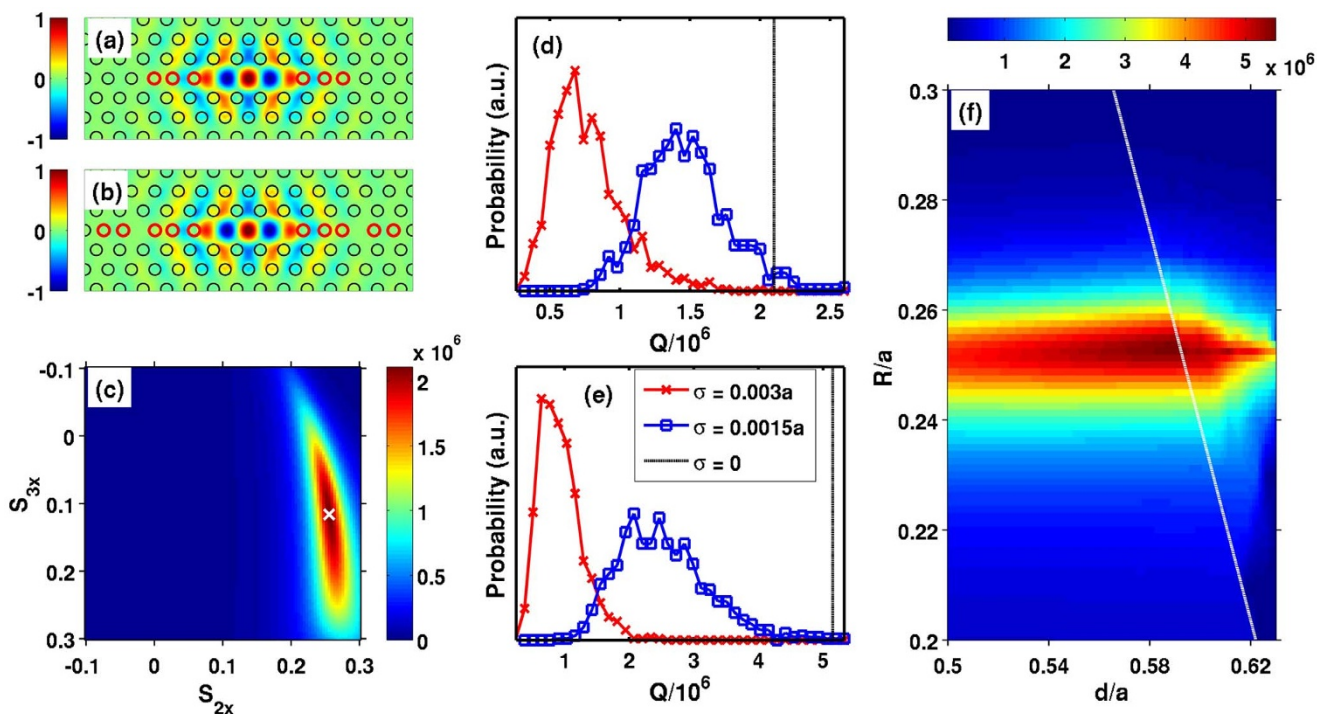
Figure 2 | (a)–(b): Electric field (E_y) profiles of the two optimized L3 designs; the holes that were displaced are marked in red. (a): $S_{1x} = 0.327a$, $S_{2x} = 0.257a$, $S_{3x} = 0.116a$. (b): $S_{1x} = 0.337a$, $S_{2x} = 0.270a$, $S_{3x} = 0.088a$, $S_{4x} = 0.323a$, $S_{5x} = 0.173a$. (c): Dependence of Q_t on S_{2x} and S_{3x} for $S_{1x} = 0.327a$; the shifts in the design of panel (a) are marked by a white cross. (d): Histograms showing the probability of occurrence of different Q_e-values in the design of panel (a), for two different disorder magnitudes: $\sigma = 0.003a$ (red) and $\sigma = 0.0015a$ (blue). The black line indicates the ideal Q_t. (e): Same as (d), for the design of (b). (f): Dependence of Q_t on the overall radius and the slab thickness, for the values of $S_{1x} - S_{5x}$ corresponding to the optimal design in (b). On the right of the dashed line, the slab becomes multi-mode at the cavity frequency.

logous trend of the loss rates as a function of R/a and d/a is expected for the other cavity designs discussed in this study. In principle, one could consider d/a and/or R/a as free parameters in the optimization, but in that case setting a target wavelength, for a fixed value of d that might arise from technological requirements, becomes more difficult.

Often, obtaining the highest possible theoretical Q_t is not the main goal of optimization. In fact, when Q_t gets above a limit set by the material and the fabrication process (currently $\approx 5 \times 10^6$ in silicon[12]), the experimentally measured Q_e is always dominated by losses due to disorder and/or absorption, and so weakly affected by further increase in Q_t. The potential of an automated optimization procedure is therefore best exploited when applied to other attractive properties. One example consists in maximizing Q_t while having the smallest possible mode volume, so that Q_t/V is as high as possible, since the latter is a figure of merit for applications in both cavity QED[25,27,28] and non-linear optics[26]. With this in mind, the second design we focus on is the H0 cavity[6,9] (sometimes also named "zero-cell" or "point-shift"), namely the simple defect cavity with the smallest known mode volume.

The design of the H0 is shown in 3(a); the defining defect is the shift of two holes away from each other (S_{1x}), the thickness of the slab taken here is $d = 0.5a$, while the hole radius is $R = 0.25a$. For the optimization, we also use the consecutive shifts $S_{2x} - S_{5x}$, as well as two shifts in the vertical direction, S_{1y} and S_{2y}. Using S_{1x}, S_{2x}, S_{3x}, S_{1y} and S_{2y}, the cavity has already been optimized[6] (following the same approach already discussed for the L3[2]) to a quality factor of $Q_t = 2.8 \times 10^5$, with a corresponding mode volume $V = 0.23(\lambda/n)^3$. Here, we improve on this result by on one hand using the genetic optimization, and on the other by including S_{4x} and S_{5x}. It should be mentioned that in the optimization, an allowed range of variation for each parameter is set. For the H0, we find that the maximum allowed S_{1x} is a

very important parameter, increasing which produces several different optimized designs. All of those are interesting, as increasing S_{1x} increases the mode volume but also the Q_t of the cavity. More precisely, the designs in 3(b)–(d) were obtained by imposing the following restrictions in the genetic algorithm: $S_{1x} \leq 0.25a$, $S_{1x} \leq 0.3a$, and $S_{1x} \leq 0.4a$, respectively. The ensuing optimal parameters [S_{1x}, S_{2x}, S_{3x}, S_{4x}, S_{5x}, S_{1y}, S_{2y}] are as follows: [0.216a, 0.103a, 0.123a, 0.004a, 0.194a, −0.017a, 0.067a] (panel (b)); [0.280a, 0.193a, 0.194a, 0.162a, 0.113a, −0.016a, 0.134a] (panel(c)); and [0.385a, 0.342a, 0.301a, 0.229a, 0.116a, −0.033a, 0.093a] (panel(d)). The corresponding quality factors are $Q_t = 1.04 \times 10^6$ (FDTD: 1.04×10^6), $Q_t = 1.88 \times 10^6$ (FDTD: 1.66×10^6), and, remarkably, $Q_t = 8.89 \times 10^6$ (FDTD: 8.29×10^6), while the respective mode volumes are $V = 0.25(\lambda/n)^3$, $V = 0.34(\lambda/n)^3$, and $V = 0.64(\lambda/n)^3$. The first among these three designs (panel (b)) has a mode volume only slightly larger than the previous most optimal design[6], combined to a quality factor almost four times larger. The last of the three designs (panel (d)) instead shows a more significant increase of the mode volume, but associated to an almost 30-fold increase of Q_t with respect to the value obtained in Ref. 6. The resonance frequencies of the three designs decrease with the increase of V and are $\frac{\omega a}{2\pi c} = 0.280$, $\frac{\omega a}{2\pi c} = 0.275$, and $\frac{\omega a}{2\pi c} = 0.269$, respectively, while the original cavity with $S_{1x} = 0.14$ (and no other shifts) of Ref. 9 has $\frac{\omega a}{2\pi c} = 0.292$.

Similarly to what we have done above for the L3 cavity, in Fig. 3(e)–(g) we present the probability of occurrence of Q_e values, computed using 1000 random disorder realizations for each design and each disorder magnitude. From these histograms it appears clearly that, even though design 3 has the highest theoretical Q_t/V, it might not be the best choice in practice. According to Eq. (1) in fact, depending on the amount of disorder, the maximum value of the
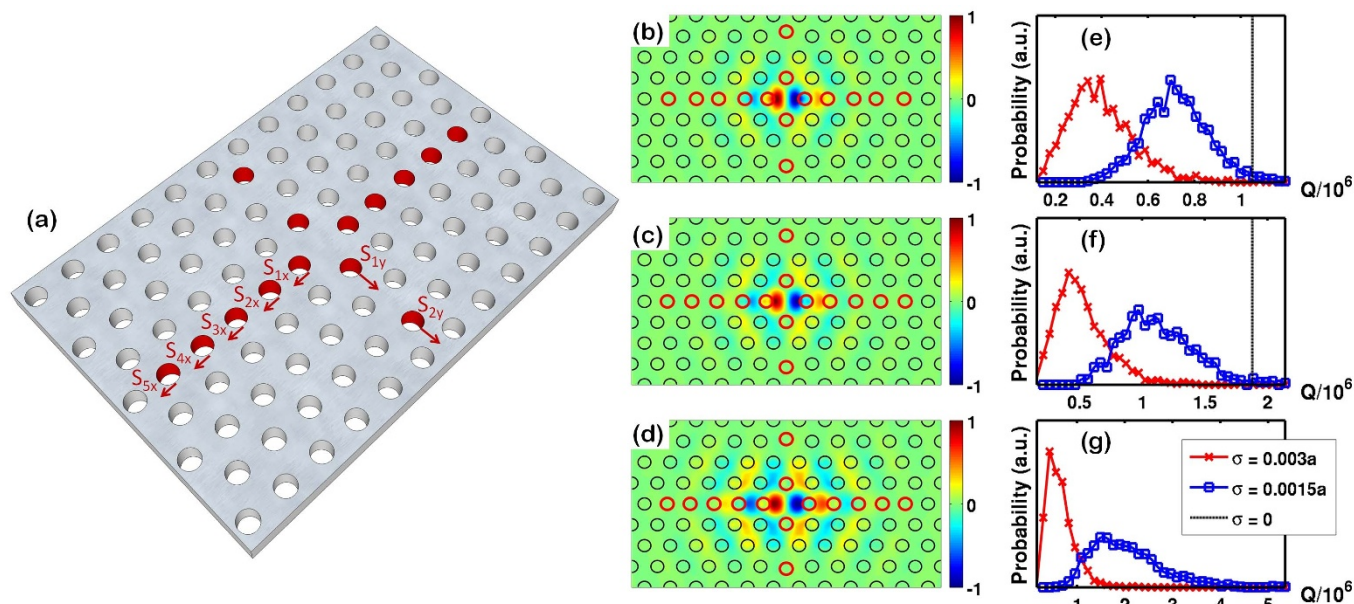
Figure 3 | (a): The design of the H0 cavity. For quality factor optimization, shifts of the positions of the five neighboring holes in the x-direction and the two neighboring holes in the y-direction were introduced, labeled as S_{1x}, S_{2x}, S_{3x}, S_{4x}, S_{5x}, S_{1y} and S_{2y} in the Figure. (b)–(d): Electric field (E_y) profiles of three optimized designs with increasing Q and V. (b): $S_{1x} = 0.216a$, $S_{2x} = 0.103a$, $S_{3x} = 0.123a$, $S_{4x} = 0.004a$, $S_{5x} = 0.194a$, $S_{1y} = -0.017a$, $S_{2y} = 0.067a$. (c): $S_{1x} = 0.280a$, $S_{2x} = 0.193a$, $S_{3x} = 0.194a$, $S_{4x} = 0.162a$, $S_{5x} = 0.113a$, $S_{1y} = -0.016a$, $S_{2y} = 0.134a$. (d): $S_{1x} = 0.385a$, $S_{2x} = 0.342a$, $S_{3x} = 0.301a$, $S_{4x} = 0.229a$, $S_{5x} = 0.116a$, $S_{1y} = -0.033a$, $S_{2y} = 0.093a$. (e): Histograms showing the probability of occurrence of different Q_e-values in the design of panel (b), for two different disorder magnitudes: $\sigma = 0.003a$ (red) and $\sigma = 0.0015a$ (blue). The black line indicates the value of Q_t. (f)–(g): Same as (e), for the designs of (c)–(d). The $\sigma = 0$ line in panel (g) is not visible as Q_t occurs beyond the axis boundary.

actual ratio Q_e/V will in general be achieved for a design having an intermediate value of Q_t. For example, in the case with $\sigma = 0.003a$ (red curves in panels (e)–(g)), the average values of Q_e (neglecting absorption) computed from the simulations are 3.97×10^5, 5.23×10^5, and 6.49×10^5, respectively, meaning that the highest Q_e/V would in practice be achieved by design 1. On the other hand, for the smaller disorder $\sigma = 0.0015a$ (blue curves in panels (e)–(g)), the corresponding average values of Q_e are 7.22×10^5, 1.12×10^6, and 2.02×10^6, and the highest average Q_e/V is achieved by design 2. For both values of σ, the expected Q_e/V for the five-shift L3 cavity is lower than that for any of the three H0 designs, thus the latter should be the cavity of choice for applications where Q/V is the most important figure of merit. We expect that design 3 will dominate for yet smaller values of σ, which however appear to be currently not achievable in practice. Additionally, design 3 could be the preferred choice for purely manufacturing reasons if quantum dots are to be inserted in the cavity, as the field maxima are further away from the hole edges than in the other two cavities. An important final remark is that cavities 1 and 2 have already been fabricated[39], and experimental quality factors consistent with the $\sigma = 0.003a$ disorder histograms have been measured (unloaded $Q_e = 485,000$ for design 2), resulting in optical bistability with ultra-low threshold power in silicon.

Another interesting cavity with potential applications for polarization-entangled photon generation[43,44] and quantum dot spin read-out[45] is the H1[9,13,34] – also known as "single point-defect cavity" – formed by one missing hole in the lattice (Fig. 4(a)). The modes of this cavity preserve the underlying hexagonal symmetry, and for a wide range of parameters, the fundamental (lowest-frequency) resonance is given by two degenerate dipole modes. Based on the electric field polarization in the center of the cavity, those are usually referred to as the y-polarized (Fig. 4 (b)) and x-polarized (Fig. 4 (c)) modes, although in fact the electric field of each of those modes also has a non-vanishing component oriented in the orthogonal direction; however, since the near-field in the very center of the cavity as well as the far-field emission in the z-direction (perpendicular to the slab

plane) are both truly y (correspondingly x) polarized, this labeling is in many cases appropriate, in particular for applications in which a quantum dot is placed in the center of the cavity. Here, we optimize the quality factor of the dipole mode. We take $d = 0.55a$ and $R = 0.23a$, and the parameters used for design optimization, labeled S_1, S_2, and S_3 in Fig. 4(a), are an increase in the side-length of the three consecutive hexagonal "rings" around the cavity (which is also equivalent to the increase of the distance from a vertex of a hexagon to the cavity center). The previously most-optimal design was achieved using only the holes at the vertices of the hexagons (but including variations of the hole radii), and has a moderate $Q_t = 6.2 \times 10^4$ and a mode volume $V = 0.47(\lambda/n)^3$[38]. Here, using the genetic algorithm with the shifts as outlined in Fig. 4(a), we find an optimal design at $S_1 = 0.213a$, $S_2 = 0.070a$, and $S_3 = -0.009a$, with $Q_t = 1.05 \times 10^6$ (FDTD: 0.97×10^6) and $V = 0.62(\lambda/n)^3$, i.e. we find a 19-fold increase in Q_t coupled to an increase in V by 32%. For this cavity as well, the disorder analysis (panel (d)) suggests that Q_e-values close to a million can be expected experimentally in state-of-the-art silicon systems, i.e. more than an order of magnitude larger than the previous *theoretical* values. The modes lie at a frequency $\frac{\omega a}{2\pi c} = 0.253$, which is, as expected, slightly lower than that of the unmodified cavity, $\frac{\omega a}{2\pi c} = 0.270$.

We note that while the degeneracy of the two dipole modes is an attractive feature of the H1, it is lifted by disorder. This is why, in panel (e) of Fig. 4, we study the probability of occurrence of the splitting between the modes, based on the 1000 disorder realizations that were used for the disorder analysis in panel (d). It is important to note that there is no absolute way to define an $x - y$ reference frame, as three equivalent frames (rotated 60° from one another) exist due to the hexagonal symmetry of the cavity. This symmetry is broken if the cavity presents preferential orientations of the axes (e.g. introduced by lithography). In the case where only random disorder is considered, x- and y-polarized modes can turn out to be oriented along either of the three $x - y$ reference frames. Thus, what we plot in panel
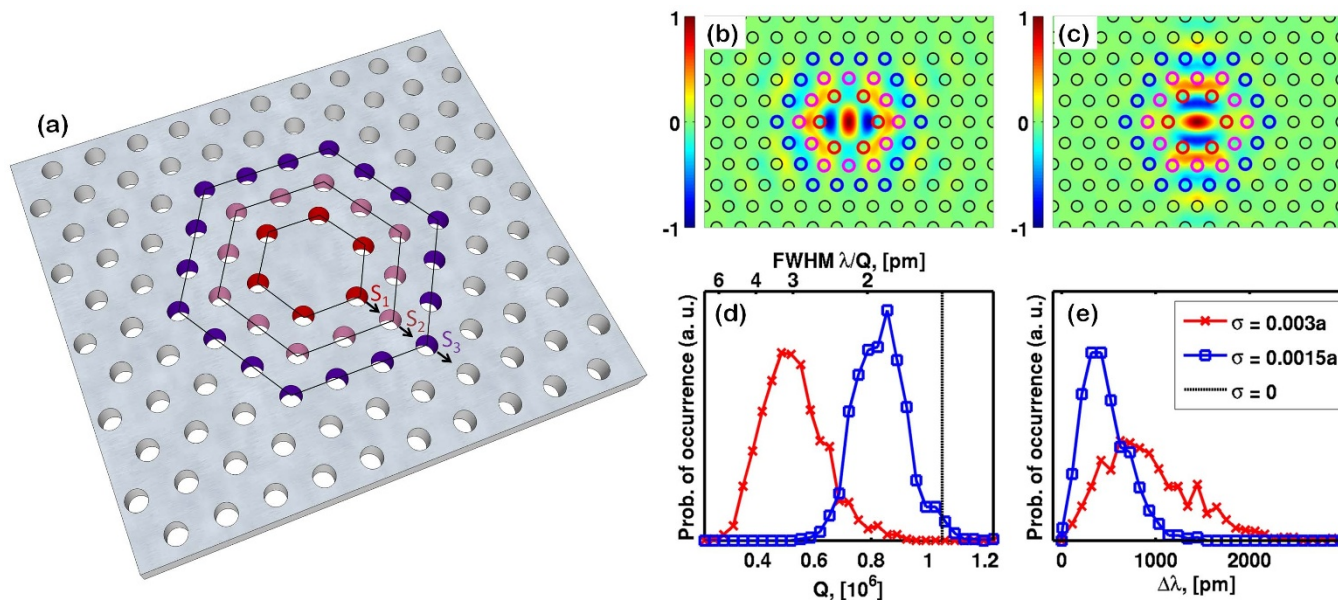
Figure 4 | (a): The design of the H1 cavity. The size of the first three hexagonal "rings" of holes is varied for quality factor optimization, with the increase of the distance from a hexagon vertex to the center of the cavity given by S_1, S_2 and S_3 (marked). (b): Electric field (E_y) profile of the y-polarized and (c): electric field (E_x) profile of the x-polarized mode, for the optimal design $S_1 = 0.213a$, $S_2 = 0.070a$, $S_3 = -0.009a$. (d): Histograms showing the probability of occurrence of different Q_e-values for two different disorder magnitudes: $\sigma = 0.003a$ (red) and $\sigma = 0.0015a$ (blue). The black line indicates the ideal Q_t. (e): Histograms showing the probability of occurrence of the wavelength splitting $\Delta\lambda$ between the two modes, which are degenerate in the disorder-less cavity.

(e) is only the difference between the resonant wavelengths of the higher- and the lower-frequency modes, without any reference to their polarization. What is important to note is that the splitting is of the order of hundreds of picometers, i.e. two orders of magnitude larger than the linewidth corresponding to the typical Q_e-s (see top x-axis of panel (d)). This implies that for applications for which overlap in frequency between the two modes is needed, some form of post-fabrication tuning is required, the possibility for which has already been demonstrated[43,46]. This can also be combined with an additional modulation of the neighboring holes which increases the emission in the vertical direction[47], which would decrease the Q_e and make the tuning easier while simultaneously increasing the intensity of the collected radiation, which is beneficial for entangled-photon generation[44,48].

We finally address the hexapole mode of the H1 cavity, that typically lies at higher frequency than the dipolar modes studied above. This mode has previously been optimized to $Q_t = 1.6 \times 10^6$ [11,13] by varying only S_1, with $S_2 = S_3 = 0$ in the sketch of Fig. 4(a). Here, we run a global optimization of Q_t by varying the three shifts, with $d = 0.55a$ and $R = 0.22a$. We could improve the previous value to $Q_t = 3.2 \times 10^6$ (FDTD: 3.1×10^6), obtained for the optimal values $S_1 = 0.271a$, $S_2 = 0.039a$, and $S_3 = 0.018a$. The resonance frequency of this mode is $\frac{\omega a}{2\pi c} = 0.261$, while in the unmodified cavity of the same d and R, this mode is not present.

The figures of merit of the seven designs that were optimized above are summarized in Table I. Notice that for the higher disorder σ_1, the values of $\langle Q_e \rangle$ do not differ dramatically among the different designs. This reflects the fact that, as has been shown in a previous analysis[37], in the disorder-dominated regime (when $Q_d \gg Q_t$), the losses are nearly design-independent.

Discussion

The designs obtained here for the three most widespread PhC defect-cavities consistently show that the quality factor of these cavities can be systematically optimized to well above 10^6 by adjusting only a few structural parameters (only shifts of hole positions were used here),

with small increases in the mode volumes (within 50% with the exception of the third H0 design) as compared to those of the corresponding non-optimized designs. In carrying out our analysis, we have tried to include the radii of holes next to the cavity as additional free parameters, but this brought no significant improvement. We therefore restricted to shifts of hole positions only, as these are easily controlled in the fabrication process. Our scheme leaves the possibility open to use the hole radii as free parameters for independent optimization of some additional figure of merit.

A very important conclusion of our analysis is that the parameter space of such structural variations has to be explored globally, using an automated optimization tool. We find that the genetic algorithm is an excellent tool to handle this task, even when seven parameters are included in the computation, as was the case for the H0 cavities. Employing this algorithm was possible only due to the computational advantage of the GME – to compute the number of cavity configurations that was needed for the optimization using a first-principle tool like FDTD or a Finite-Element Method (FEM) would require either an enormous computational power, or time of the order of years. This computational advantage made it also possible, for each cavity type, to vary more structural parameters than in previous optimization works, thus bringing to an even larger increase in the quality factors. Finally, we note that the GME returns not only the quality factor but also the full mode profile of the cavity modes, thus the same procedure which was presented here can be used for optimization of different quantities depending on the practical requirements, like Q/V for applications in non-linear optics, or optimal electric field profiles for e.g. sensing technologies[23], which we expect to explore in the next future.

The statistical analysis of Q-factors including structural disorder shows clearly that the designs obtained here are as robust to disorder as other ultrahigh-Q designs[37]. In particular, for the L3 cavity with a theoretical Q-factor $Q_t = 5.1 \times 10^6$, state-of-the-art fabrication quality in silicon should easily result in experimental Q-factors around 2×10^6, in the same range as current ultrahigh-Q designs based on a PhC waveguide[10–12]. On the other hand, our experience shows that systematic structural variations can rapidly suppress the Q-factor of

Table I | Summary of the simulated resonant frequency, quality factor, mode volume, and Q/V ratio for the seven optimal designs studied in this work. The last four columns list average values computed over 1000 disorder realizations, in which both hole radii and position are subject to Gaussian fluctuations with standard deviation $\sigma_1 = 0.003a$ and $\sigma_2 = 0.0015a$

Cavity	$\frac{\omega a}{2\pi c}$	Q_t	$V, \left(\frac{\lambda}{n}\right)^3$	$\frac{Q_t}{V}, \left(\frac{n}{\lambda}\right)^3$	$\langle Q_e\rangle_{\sigma_1}$	$\frac{\langle Q_e\rangle_{\sigma_1}}{V}, \left(\frac{n}{\lambda}\right)^3$	$\langle Q_e\rangle_{\sigma_2}$	$\frac{\langle Q_e\rangle_{\sigma_2}}{V}, \left(\frac{n}{\lambda}\right)^3$
L3 des. 1	0.259	2.1×10^6	0.94	2.2×10^6	0.77×10^6	0.82×10^6	1.5×10^6	1.6×10^6
L3 des. 2	0.259	5.1×10^6	0.95	5.4×10^6	0.93×10^6	0.98×10^6	2.5×10^6	2.6×10^6
H0 des. 1	0.280	1.0×10^6	0.25	4.2×10^6	0.40×10^6	1.6×10^6	0.72×10^6	3.0×10^6
H0 des. 2	0.275	1.9×10^6	0.35	5.4×10^6	0.52×10^6	1.5×10^6	1.1×10^6	3.1×10^6
H0 des. 3	0.269	8.9×10^6	0.64	14×10^6	0.65×10^6	1.0×10^6	2.0×10^6	3.1×10^6
H1 dip.	0.253	1.0×10^6	0.62	1.6×10^6	0.53×10^6	0.85×10^6	0.84×10^6	1.4×10^6
H1 hexap.	0.261	3.2×10^6	1.1	2.9×10^6	0.66×10^6	0.60×10^6	1.6×10^6	1.5×10^6

an optimal structure. Hence, an important conclusion of our analysis is that, whenever a design needs to be significantly varied (e.g. when strongly modifying the ratios R/a and/or d/a, or the refractive index n in order to, e.g., operate at a different wavelength), *a new optimization must be carried out* in order to obtain the best structural design adapted to the new requirements.

The range of applicability of the present scheme is very broad. We are currently applying it to several systems, including the optimization of the Q-factor of PhC cavities with low index contrast[49], of cavities based on a thicker slab ($d/a > 1$, typically needed to host some quantum nanostructures[50]), but also to the maximization of the trapping capabilities of slot cavities designed for biological sensing[23], and to the simultaneous optimization of first and second order modes of a cavity built in a PhC structure with doubly resonant bandgap for efficient second-harmonic generation[51]. In all these cases, the global optimization brought to very promising results. A further application might include the optimization of PhC structures based on a silicon-on-insulator design[52,53]. Perhaps even more importantly, our work has general implications about the future research in photonic crystals, as it shows that the domain of possible structural designs is still largely unexplored, while simultaneously demonstrating how its exploration can be done efficiently.

Methods

The guided-mode expansion. The GME method used in this work[38] is based on expanding the mode of a cavity on the basis of the guided modes of an effective dielectric slab. In the z-direction (orthogonal to the slab plane), the whole space from minus to plus infinity is included analytically; in the slab plane, a finite super-cell is taken and periodic boundary conditions are assumed. The super-cell size in our simulations ranges from $L_x = 16a$ to $L_x = 20a$ in the x-direction and from $L_y = 12\left(\sqrt{3}a/2\right)$ to $L_y = 20\left(\sqrt{3}a/2\right)$ in the y-direction, depending on the cavity. The supercell naturally defines a grid of in-plane wave-vectors $\mathbf{G} = 2\pi(n_x/L_x, n_y/L_y)$ (with integer n_x and n_y), each of them labeling a wave guided inside the slab and evanescent along the z-direction. The expansion is carried out onto a truncated set of N_G such waves (centered at $\mathbf{G} = 0$) and the number N_G is increased until convergence is reached (typically $N_G \geq 5000$). For all the optimizations, only the fundamental ($\alpha = 1$ in Ref. 38) guided mode is used, since for the thickness assumed here, the admixture of higher guided modes is negligible at the cavity resonant frequencies. In the multi-mode region of Fig. 2(f), the second ($\alpha = 2$) guided mode is also included. To correct for a small systematic offset in the quality factor Q_t due to the periodic boundary conditions, an averaging of the losses of the Bloch modes of the cavity over a grid in k-space containing 10 to 20 points is performed. With these numerical parameters, obtaining the Q for a given cavity configuration takes of the order of five minutes using one processor and 2 GB of RAM. When the slab becomes multi-mode, the distribution of losses in k-space presents a sharp, narrow peak around the k values for which the cavity mode is exactly in resonance with the TM-like band of the regular PhC[38]. In that case a finer grid (or numerical integration) in k-space is needed to correctly compute the quality factor, and simulating one cavity configuration takes of the order of a few hours with the same computational resources.

FDTD simulations. For the FDTD simulations, we use the freely available MIT Electromagnetic Equation Propagation (MEEP) package[40]. Typical simulations parameters are supercell size $40a$ in the x-direction and $30\left(\sqrt{3}a/2\right)$ in the y-direction, and spatial resolution $20/a$. Taking advantage of the parallelized (MPI) version of the software, a converged computation takes of the order of ten hours on a 16-core processor with 32 GB of RAM. A more detailed comparison of

computational time and accuracy between GME, FDTD and the Finite-Element Method (FEM) can be found in Ref. 37.

Genetic optimization. The implementation of the genetic algorithm included in the Global Optimization Toolbox (MATLAB and Global Optimization Toolbox Release 2012b, The MathWorks, Inc., Natick, Massachusetts, United States), which starts from a random initial population (i.e. a set of points in parameter space) and goes on to create a sequence of generations (new sets of such points) where the 'fittest' individuals are kept. The algorithm incorporates an array of evolutionary inspired techniques, including cross-over, random mutations, and natural selection of individuals. An 'individual' in our case is simply one Q-computation for a particular set of cavity parameters, and the higher the quality factor, the higher the assigned 'fitness' of the individual (i.e. its probability to survive to the next generation and/or to be mixed with another individual to produce an 'offspring' lying in parameter space somewhere in between the two). With the increase of the number of free parameters, the number of generations needed for convergence increases. In the presented work, the maximum is reached for the H0 cavity with 7 parameters, for which ≈ 300 generations each consisting of 120 individuals are needed for convergence. This can however be greatly improved if a rough optimization is first carried out (with a large allowed range for the free parameters), followed by a finer optimization centered around the rough maximum. The longest optimization we ran thus took about a week on twelve CPUs with 32 GB of RAM. This would have taken more than ten years to finish using the same machine but employing an FDTD solver instead of the GME.

Mode volume. Here we adopt the definition of the mode volume that is most commonly used to quantify the performance of a nanocavity:

$$V = \frac{\int \varepsilon(\mathbf{r})|\mathbf{E}(\mathbf{r})|^2 d^3 r}{\max\left[\varepsilon(\mathbf{r})|\mathbf{E}(\mathbf{r})|^2\right]}. \qquad (2)$$

This definition is the one needed in cavity quantum electrodynamics as a measure of the radiation-matter coupling with a pointlike two-level system placed at the position where the field intensity has a maximum. Other definitions are more suited to different purposes and might in some cases differ dramatically from the one above[11].

1. Akahane, Y., Asano, T., Song, B. & Noda, S. High-q photonic nanocavity in a two-dimensional photonic crystal. *Nature* **425**, 944–947 (2003).
2. Akahane, Y., Asano, T., Song, B.-S. & Noda, S. Fine-tuned high-q photonic-crystal nanocavity. *Opt. Express* **13**, 1202–1214 (2005).
3. Englund, D., Fushman, I. & Vuckovic, J. General recipe for designing photonic crystal cavities. *Opt. Express* **13**, 5961–5975 (2005).
4. Felici, M., Atlasov, K. A., Surrente, A. & Kapon, E. Semianalytical approach to the design of photonic crystal cavities. *Phys. Rev. B* **82**, 115118 (2010).
5. Kuramochi, E. *et al.* Ultrahigh-q photonic crystal nanocavities realized by the local width modulation of a line defect. *Appl. Phys. Lett.* **88**, 041112 (2006).
6. Nomura, M., Tanabe, K., Iwamoto, S. & Arakawa, Y. High-q design of semiconductor-based ultrasmall photonic crystal nanocavity. *Opt. Express* **18**, 8144–8150 (2010).
7. Song, B., Noda, S., Asano, T. & Akahane, Y. Ultra-high-q photonic double-heterostructure nanocavity. *Nature Mater.* **4**, 207–210 (2005).
8. Takagi, H. *et al.* High q h1 photonic crystal nanocavities with efficient vertical emission. *Opt. Express* **20**, 28292–28300 (2012).
9. Zhang, Z. & Qiu, M. Small-volume waveguide-section high q microcavities in 2 d photonic crystal slabs. *Opt. Express* **12**, 3988–3995 (2004).
10. Han, Z. *et al.* Optimized design for 2 106 ultra-high q silicon photonic crystal cavities. *Opt. Commun.* **283**, 4387–4391 (2010).
11. Notomi, M. Manipulating light with strongly modulated photonic crystals. *Rep. Prog. Phys.* **73**, 096501 (2010).
12. Taguchi, Y., Takahashi, Y., Sato, Y., Asano, T. & Noda, S. Statistical studies of photonic heterostructure nanocavities with an average q factor of three million. *Opt. Express* **19**, 11916–11921 (2011).

13. Tanabe, T. *et al.* Single point defect photonic crystal nanocavity with ultrahigh quality factor achieved by using hexapole mode. *Appl. Phys. Lett.* **91**, 021110 (2007).

14. Tanabe, T., Notomi, M., Kuramochi, E., Shinya, A. & Taniyama, H. Trapping and delaying photons for one nanosecond in an ultrasmall high-q photonic-crystal nanocavity. *Nature Photon.* **1**, 49–52 (2007).

15. Faraon, A. *et al.* Coherent generation of non-classical light on a chip via photon-induced tunnelling and blockade. *Nature Phys.* **4**, 859–863 (2008).

16. Husko, C. *et al.* Ultrafast all-optical modulation in GaAs photonic crystal cavities. *Appl. Phys. Lett.* **94**, 021111 (2009).

17. Dorfner, D. *et al.* Photonic crystal nanostructures for optical biosensing applications. *Biosens. Bioelectron.* **24**, 3688–3692 (2009).

18. Nozaki, K. *et al.* Sub-femtojoule all-optical switching using a photonic-crystal nanocavity. *Nature Photon.* **4**, 477–483 (2010).

19. Nozaki, K. *et al.* Ultralow-power all-optical ram based on nanocavities. *Nature Photon.* **6**, 248–252 (2012).

20. Sato, Y. *et al.* Strong coupling between distant photonic nanocavities and its dynamic control. *Nature Photon.* **6**, 56–61 (2012).

21. Reinhard, A. *et al.* Strongly correlated photons on a chip. *Nature Photon.* **6**, 93–96 (2012).

22. Volz, T. *et al.* Ultrafast all-optical switching by single photons. *Nature Photon.* **6**, 605–609 (2012).

23. Descharmes, N., Dharanipathy, U. P., Diao, Z., Tonin, M. & Houdré, R. Observation of backaction and self-induced trapping in a planar hollow photonic crystal cavity. *Phys. Rev. Lett.* **110**, 123601 (2013).

24. Priolo, F., Gregorkiewicz, T., Galli, M. & Krauss, T. F. Silicon nanostructures for photonics and photovoltaics. *Nature Nanotech.* **9**, 19–32 (2014).

25. Andreani, L. C., Panzarini, G. & Grard, J.-M. Strong-coupling regime for quantum boxes in pillar microcavities: Theory. *Phys. Rev. B* **60**, 13276–13279 (1999).

26. Barclay, P., Srinivasan, K. & Painter, O. Nonlinear response of silicon photonic crystal microresonators excited via an integrated waveguide and fiber taper. *Opt. Express* **13**, 801–820 (2005).

27. Englund, D. *et al.* Controlling the spontaneous emission rate of single quantum dots in a two-dimensional photonic crystal. *Phys. Rev. Lett.* **95**, 013904 (2005).

28. Yoshie, T. *et al.* Vacuum rabi splitting with a single quantum dot in a photonic crystal nanocavity. *Nature* **432**, 200–203 (2004).

29. Jensen, J. & Sigmund, O. Topology optimization for nano-photonics. *Laser Photon. Rev.* **5**, 308–321 (2011).

30. Frei, W. R., Johnson, H. T. & Choquette, K. D. Optimization of a single defect photonic crystal laser cavity. *J. Appl. Phys.* **103**, – (2008).

31. Liang, X. & Johnson, S. G. Formulation for scalable optimization of microcavities via the frequency-averaged local density of states. *Opt. Express* **21**, 30812 (2013).

32. Wang, D. *et al.* Ultrasmall modal volume and high q factor optimization of a photonic crystal slab cavity. *J. Opt.* **15**, 125102 (2013).

33. Saucer, T. W. & Sih, V. Optimizing nanophotonic cavity designs with the gravitational search algorithm. *Opt. Express* **21**, 20831–20836 (2013).

34. Painter, O., Vučković, J. & Scherer, A. Defect modes of a two-dimensional photonic crystal in an optically thin dielectric slab. *J. Opt. Soc. Am. B* **16**, 275–285 (1999).

35. Portalupi, S. L. *et al.* Deliberate versus intrinsic disorder in photonic crystal nanocavities investigated by resonant light scattering. *Phys. Rev. B* **84**, 045423 (2011).

36. Hagino, H., Takahashi, Y., Tanaka, Y., Asano, T. & Noda, S. Effects of fluctuation in air hole radii and positions on optical characteristics in photonic crystal heterostructure nanocavities. *Phys. Rev. B* **79**, 085112 (2009).

37. Minkov, M., Dharanipathy, U. P., Houdré, R. & Savona, V. Statistics of the disorder-induced losses of high-q photonic crystal cavities. *Opt. Express* **21**, 28233–28245 (2013).

38. Andreani, L. C. & Gerace, D. Photonic-crystal slabs with a triangular lattice of triangular holes investigated using a guied-mode expansion method. *Phys. Rev. B* **73**, 235114 (2006).

39. Dharanipathy, U. P., Minkov, M., Tonin, M., Savona, V. & Houdré, R. Evolutionarily optimized ultrahigh-q photonic crystal nanocavity. *arXiv:1311.0997 [cond-mat, physics:physics]* (2013).

40. Oskooi, A. F. *et al.* MEEP: A flexible free-software package for electromagnetic simulations by the FDTD method. *Comput. Phys. Commun.* **181**, 687–702 (2010).

41. Minkov, M. & Savona, V. Effect of hole-shape irregularities on photonic crystal waveguides. *Opt. Lett.* **37**, 3108–3110 (2012).

42. Le Thomas, N., Diao, Z., Zhang, H. & Houdré, R. Statistical analysis of subnanometer residual disorder in photonic crystal waveguides: Correlation between slow light properties and structural properties. *J. Vac. Sci. Technol., B* **29**, 051601 (2011).

43. Hennessy, K., Hogerle, C., Hu, E., Badolato, A. & Imamoglu, A. Tuning photonic nanocavities by atomic force microscope nano-oxidation. *Appl. Phys. Lett.* **89**, 041118 (2006).

44. Larque, M., Karle, T., Robert-Philip, I. & Beveratos, A. Optimizing h1 cavities for the generation of entangled photon pairs. *New J. Phys.* **11**, 033022 (2009).

45. Coles, R. J. *et al.* Waveguide-coupled photonic crystal cavity for quantum dot spin readout. *arXiv:1310.7848 [physics]* (2013).

46. Luxmoore, I. J., Ahmadi, E. D., Fox, A. M., Hugues, M. & Skolnick, M. S. Unpolarized h1 photonic crystal nanocavities fabricated by stretched lattice design. *Appl. Phys. Lett.* **98**, – (2011).

47. Portalupi, S. L. *et al.* Planar photonic crystal cavities with far-field optimization for high coupling efficiency and quality factor. *Opt. Express* **18**, 16064–16073 (2010).

48. Hagemeier, J. *et al.* H1 photonic crystal cavities for hybrid quantum information protocols. *Opt. Express* **20**, 24714–24726 (2012).

49. Dharanipathy, U. *et al.* Near-infrared characterization of gallium nitride photonic-crystal waveguides and cavities. *Opt. Lett.* **37**, 4588–4590 (2012).

50. Surrente, A. *et al.* Ordered systems of site-controlled pyramidal quantum dots incorporated in photonic crystal cavities. *Nanotechnology* **22**, 465203 (2011).

51. Rivoire, K., Lin, Z., Hatami, F., Masselink, W. T. & Vučković, J. Second harmonic generation in gallium phosphide photonic crystal nanocavities with ultralow continuous wave pump power. *Opt. Express* **17**, 22609–22615 (2009).

52. Han, Z., Checoury, X., Haret, L.-D. & Boucaud, P. High quality factor in a two-dimensional photonic crystal cavity on silicon-on-insulator. *Opt. Lett.* **36**, 1749–1751 (2011).

53. Tanaka, Y., Asano, T., Hatsuta, R. & Noda, S. Investigation of point-defect cavity formed in two-dimensional photonic crystal slab with one-sided dielectric cladding. *Appl. Phys. Lett.* **88**, – (2006).

Acknowledgments

Author contributions

M.M. and V.S. contributed equally to obtaining the results and writing the manuscript.

Additional information